ACS Photonics

Article

Cite This: ACS Photonics 2018, 5, 1101−1107

Antimatched Electromagnetic Metasurfaces for Broadband Arbitrary Phase Manipulation in Reflection

Odysseas Tsilipakos,*[,†] Thomas Koschny,[‡] and Costas M. Soukoulis[†,‡]

[†]Institute of Electronic Structure and Laser, FORTH, GR-71110 Heraklion, Crete, Greece

[‡]Ames Laboratory—U.S. DOE and Department of Physics and Astronomy, Iowa State University, Ames, Iowa 50011, United States

Supporting Information

ABSTRACT: Metasurfaces impart phase discontinuities on impinging electromagnetic waves that are typically limited to 0−2π. Here, we demonstrate that multiresonant metasurfaces can break free from this limitation and supply arbitrarily large, tunable time delays over ultrawide bandwidths. As such, ultrathin metasurfaces can act as the equivalent of thick bulk structures by emulating the multiple geometric resonances of three-dimensional systems that originate from phase accumulation with effective material resonances implemented on the surface itself via suitable subwavelength meta-atoms. We describe a constructive procedure for defining the required sheet admittivities of such metasurfaces. Importantly, the proposed approach provides an exactly linear phase response so that broadband pulses can experience the desired group delay without any distortion of the pulse shape. We focus on operation in reflection by exploiting an antimatching condition, satisfied by interleaved electric and magnetic Lorentzian resonances in the surface admittivities, which completely zeroes out transmission through the metasurface. As a result, the proposed metasurfaces can perfectly reflect a broadband pulse imparting a prescribed group delay. The group delay can be tuned by modifying the implemented resonances, thus opening up diverse possibilities in the temporal applications of metasurfaces.

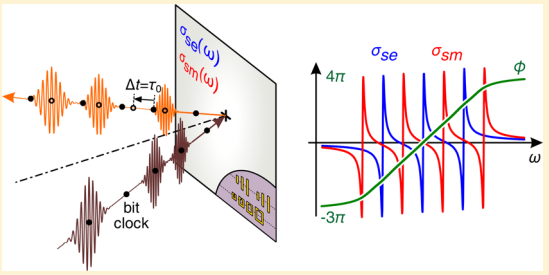

KEYWORDS: *metasurfaces, metamaterials, multiple resonances, tunable, broadband, reflection, phase delay, group delay*

Metasurfaces are the two-dimensional versions of metamaterials, typically formed by arranging subwavelength resonant meta-atoms on a single plane. They have been investigated intensely in recent years for an abundance of functionalities spanning perfect absorption,[1,2] dispersion compensation,[3] electromagnetically induced transparency,[4] wavefront transformations,[5−21] polarization control,[22,23] and nonreciprocal response.[24,25] Operation in both transmission and reflection has been examined, and the main achievements can be found in recent review papers.[26−29]

An important realization along the way has been that metasurfaces with both electric and magnetic response can extend the π phase span offered by purely electric resonant sheets and provide a phase modulation approaching 2π. This, by Huygens' principle, allows for full control over the wavefront; at the same time, the excitation of both electric and magnetic surface currents allows for unidirectional scattering. Thus, impedance-matched gradient metasurfaces that provide maximum efficiency in transmission and perform prescribed wavefront transformations became possible.[7] Still, even electromagnetic sheets exhibit a limited delay-bandwidth product, restricted by the maximum 2π shift obtained over the narrow bandwidth of the matched resonance pair.

In this work, we demonstrate that metasurfaces can overcome this longstanding limitation and provide arbitrarily large time delays over broad bandwidths. This is achieved by implementing *multiple*, properly arranged resonances in the effective surface admittivities. As such, ultrathin metasurfaces can act as the equivalent of thick bulk structures, by emulating the multiple geometric (e.g., Fabry−Pérot) resonances of three-dimensional systems that originate from phase accumulation with effective material resonances on the surface itself via suitable subwavelength meta-atoms. Both electric and magnetic resonances are necessary for obtaining control over unidirectional radiation. Importantly, we require flat amplitude response and an exactly linear phase profile corresponding to zero group delay dispersion. As a result, broadband pulses can interact with the metasurface and experience the desired group delay with zero pulse distortion. The group delay can be readily tuned (or switched off) by modifying (quenching) the implemented resonances, thus opening up diverse possibilities in the temporal applications of metasurfaces.

We focus on operation in reflection mode, drawing on an idea introduced in ref 30 for operation in transmission. Operating in reflection is highly desirable for the tunable delay applications since any control circuitry for tuning the implemented resonances can be accommodated behind the metasurface without interfering with the electromagnetic wave. Notably, efficient operation in reflection is achieved by exploiting an admittivity antimatching condition which zeroes

Received: November 23, 2017
Published: January 3, 2018

DOI: 10.1021/acsphotonics.7b01415
ACS Photonics 2018, 5, 1101−1107

out transmission. As a result, the proposed metasurfaces are highly efficient with power lost only through absorption.

CREATING A MONOTONIC ACCUMULATIVE REFLECTION PHASE

In ultrathin metasurfaces where geometric resonances are absent, phase delay can only be provided by effective material resonances, i.e., those of the constituent meta-atoms. For arbitrarily large delays one needs to break free from the typical singly resonant metasurfaces and enter the multiresonant regime. Our first concern is to determine the proper way of arranging multiple resonances so that the respective phase shifts combine constructively, producing a monotonic aggregate phase shift.

Let us consider a metasurface described by electric and magnetic surface admittivities (complex conductivities) σ_{se} and σ_{sm} measured in S and Ω, respectively.[31] We assume that the macroscopic admittivities are the result of homogenized microscopic meta-atom responses and can feature multiple Lorentzian resonances. The equations relating the surface admittivities with reflection and transmission coefficients are[32,33]

$$r(\omega, \theta) = \frac{-\tilde{\sigma}_{se} + \tilde{\sigma}_{sm}}{1 + \tilde{\sigma}_{se}\tilde{\sigma}_{sm} + \tilde{\sigma}_{se} + \tilde{\sigma}_{sm}} \tag{1a}$$

$$t(\omega, \theta) = \frac{1 - \tilde{\sigma}_{se}\tilde{\sigma}_{sm}}{1 + \tilde{\sigma}_{se}\tilde{\sigma}_{sm} + \tilde{\sigma}_{se} + \tilde{\sigma}_{sm}} \tag{1b}$$

$$\tilde{\sigma}_{se}(\omega, \theta) = \frac{\zeta\sigma_{se}}{2} = \frac{1 - r - t}{1 + r + t} \tag{2a}$$

$$\tilde{\sigma}_{sm}(\omega, \theta) = \frac{\sigma_{sm}}{2\zeta} = \frac{1 + r - t}{1 - r + t} \tag{2b}$$

where we have defined dimensionless *effective* admittivities $\tilde{\sigma}_{se}(\omega, \theta) = \zeta\sigma_{se}/2$ and $\tilde{\sigma}_{sm}(\omega, \theta) = \sigma_{sm}/(2\zeta)$. Note that $\zeta^{TE}(\theta) = \omega\mu/k_{\perp} = \eta\ \sec(\theta)$ and $\zeta^{TM}(\theta) = k_{\perp}/(\omega\varepsilon) = \eta\ \cos(\theta)$ for the TE and TM polarization, respectively, where θ is the incidence angle and $\eta = \sqrt{\mu/\varepsilon}$ is the characteristic impedance of the homogeneous host medium. Both r and t as well as $\tilde{\sigma}_{se}$ and $\tilde{\sigma}_{sm}$ depend on the polarization, with the notation suppressed for brevity.

A single resonance in the electric or magnetic surface admittivity results in a spectral region of high reflection and an underlying π phase variation. The bandwidth of high reflection is limited, being directly associated with the resonance linewidth. Trying to increase the bandwidth and the available phase span, one could think of placing two resonances of the same kind (electric or magnetic) side by side (Figure 1a). However, the resonances do not combine in a single high-reflection region. The respective susceptivity (imaginary part of admittivity) contributions compensate each other approximately halfway between the two resonant frequencies. At the zero crossing we get a reflection zero since no currents are induced on the metasurface. Importantly, while traversing the zero crossing, the polarization shifts from antiphase to in-phase and the reflection phase from $3\pi/2$ to $\pi/2$ ($E_{ref} \propto J_{se} \propto \dot{P}_{se}$). Thus, the reflection phase is not monotonic and respective π shifts do not add up to 2π.

Reflection phase monotonicity can be achieved by utilizing adjacent resonances of different kind (Figure 1b). Since electric and magnetic susceptivities cannot compensate each other, the

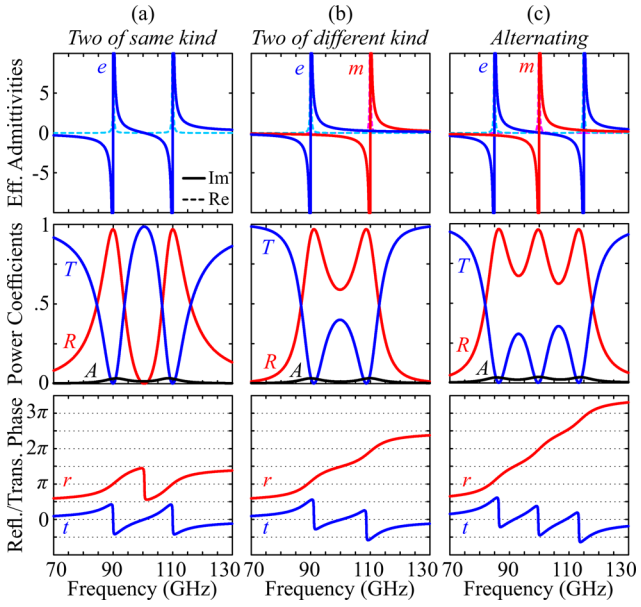

Figure 1. Metasurface with resonant surface admittivities. (a) Adjacent resonances of the same kind (electric). The susceptivity zero crossing leads to a reflection minimum. The reflection phase is not monotonic. (b) Adjacent electric and magnetic resonances. Electric and magnetic susceptivities cannot compensate each other, and the reflection phase is monotonic. (c) Alternating electric and magnetic resonances. The magnetic resonance masks the electric susceptivity zero crossing. The reflection zero is avoided, and the reflection phase is monotonic. For the parameters of the Lorentzian resonances see the Supporting Information.

reflection phase becomes monotonic and respective π shifts add up to 2π. Moreover, by avoiding the zero crossing and the associated reflection zero we end up with a single high-reflection region. This concept can be generalized to multiple resonances despite the fact that susceptivity zero crossings will be inevitably present. Consider for example alternating electric, magnetic, electric resonances (Figure 1c). Although there is a zero crossing in the electric susceptivity, it is masked by the magnetic resonance and the associated reflection zero is avoided. As a result, the reflection phase is monotonic and respective π shifts add up to 3π. Note that out of the available 3π span more than 2π is obtained under high reflection. Thus, Figure 1c illustrates a way of achieving a 2π span in reflection using passive isotropic metasheets. This can be exploited in designing gradient metasurfaces in reflection, presenting an alternative to magnetoelectric coupling[13] or structures with a ground plane.[10,11] Three resonances are required in contrast to the transmission case, where two matched electric and magnetic resonances provide the entire 2π shift under high transmission.

BROADBAND UNIFORM REFLECTION WITH ZERO GROUP DELAY DISPERSION

We now seek to build on the concept of alternating resonances. Our goal is to perfectly reflect broadband pulses imparting on them a tunable time delay. Observing Figure 1c, we recognize that the reflection bandwidth is finite, the amplitude is not flat, and the phase is not linear. To accommodate arbitrarily broadband pulses without any pulse distortion, we need wideband flat reflection with zero group delay dispersion. Mathematically, we require $r(\omega) = -\mathcal{A}\exp(i\tau_0\omega)$ and $t(\omega) = 0$ for the scattering amplitudes of the metasurface, where τ_0 is

DOI: 10.1021/acsphotonics.7b01415
ACS Photonics 2018, 5, 1101−1107

the desired group delay and the prefactor $\mathcal{A}$ allows for some absorption in the metasurface.[34] Substituting this mathematical prescription in eq 2 we find

$$\tilde{\sigma}_{se} = \frac{1}{\tilde{\sigma}_{sm}} = \frac{1 + \mathcal{A}e^{i\tau_0\omega}}{1 - \mathcal{A}e^{i\tau_0\omega}} \tag{3}$$

stating that the surface admittivities should exhibit a specific frequency dependence while being complex inverses. Notice that the poles of $\tilde{\sigma}_{se}$ coincide with the zeros of $\tilde{\sigma}_{sm}$ and vice versa, in agreement with the concept of interleaved resonances guaranteeing a monotonic accumulative reflection phase. Importantly, in analogy with the well-known admittivity matching condition $\tilde{\sigma}_{se} = \tilde{\sigma}_{sm}$[7] which zeroes-out reflection, eq 1a, there is an *antimatching* condition $\tilde{\sigma}_{se} = 1/\tilde{\sigma}_{sm}$ that zeroes out transmission, eq 1b. This condition has been identified independently in refs 35 and 36, albeit exploited for a single frequency point.

Equation 3 describes the target spectrum. However, only certain types of resonant behavior are available in nature. Thus, we seek a good approximation of the target spectrum using Lorentzian resonances, which can be provided by subwavelength meta-atoms. Using a partial fraction decomposition at the poles of eq 3, as detailed in the Supporting Information, we end up with a *physical* recipe that matches the target spectrum almost perfectly. It requires trains of interleaved electric and magnetic Lorentzian resonances with proper frequency spacing, strength (κ), and damping (Γ):

$$\tilde{\sigma}_{se} = \frac{i\kappa_e/2}{\omega + i\Gamma_e^{cor}/2} + \sum_{k=1}^{+\infty} \frac{i\kappa_e\omega}{\omega^2 - \omega_{e,k}^2 + i\Gamma_e\omega} \tag{4a}$$

$$\tilde{\sigma}_{sm} = \sum_{k=0}^{+\infty} \frac{i\kappa_m\omega}{\omega^2 - \omega_{m,k}^2 + i\Gamma_m\omega} \tag{4b}$$

where $\omega_{e,k} = [(2k\pi)^2 + \ln^2(\mathcal{A})]^{1/2}/\tau_0$ with $k = 1, 2, ...$, $\omega_{m,k} = \{[(2k+1)\pi]^2 + \ln^2(\mathcal{A})\}^{1/2}/\tau_0$ with $k = 0, 1, 2, ...$, $\kappa_e = \kappa_m = 4/\tau_0$, $\Gamma_e = \Gamma_m = 2|\ln(\mathcal{A})|/\tau_0$, and $\Gamma_e^{cor} = [2(1-\mathcal{A})/(\mathcal{A}|\ln(\mathcal{A})|)]\Gamma_e$. Physically, the interleaved resonances guarantee the monotonicity of the reflection phase, as illustrated in Figure 1c. The specific frequency spacing, strength, and damping are required for providing uniform reflection and a linear phase response. The only input parameters of the recipe are the desired group delay τ_0 and the allowed attenuation in the metasurface $\mathcal{A}$. For large (of practical interest) values of $\mathcal{A}$ the normalized ($\tilde{\omega} \triangleq \omega\tau_0/\pi$) electric and magnetic resonant frequencies are given by $\tilde{\omega}_{e,k} \approx 2k$ (even integers) and $\tilde{\omega}_{m,k} \approx 2k + 1$ (odd integers), respectively. This can be seen in Figure 2a, where we plot the recipe for $\mathcal{A} = 0.9$ in the spectral region $\tilde{\omega} = 0...8$, involving the first four electric and magnetic resonances. Notice that the $k = 0$ (Drude) electric term is characterized by a different damping frequency Γ_e^{cor} as evidenced by the peaking of $\mathrm{Im}(\tilde{\sigma}_{se})$ at ~5 instead of ~10.

The response of the recipe is plotted in Figure 2b by substituting eq 4 into eq 1. Reflection $R = |r|^2$ is flat and equal to the prescribed $\mathcal{A}^2 = 0.81$. This behavior extends to arbitrarily high frequencies for the untruncated sums of eq 4. Transmission is zero since we have satisfied the antimatching condition. Notice the effect of the Drude term correction meant to provide proper loss at DC (see Supporting Information). Importantly, the phase is exactly linear. Physically, this relies on characteristic points with $\mathrm{Arg}(r) = \mp\pi/2$ showing up at the midpoints between resonances ($\tilde{\omega} \approx k + 1/2$). Then, starting from an electric resonant frequency the reflection phase *equidistantly* traverses $\{-\pi, -\pi/2, 0, +\pi/2, +\pi, ...\}$, leading to a linear phase response. Note that $\mathrm{Arg}(r) = \mp\pi/2$ is attained when $|\tilde{\sigma}_s| = 1$ and the admittivities have negative-equal imaginary parts: $\tilde{\sigma}_{se} = \pm ia + b$ and $\tilde{\sigma}_{sm} = 1/\tilde{\sigma}_{se} = \mp ia + b$. Substituting in eq 1a one finds $r = \mp ia/(1+b)$, i.e., $\mathrm{Arg}(r) = \mp\pi/2$. For $\mathcal{A}$ values of practical interest the admittivity real parts are small at the midpoints, leading to $a \approx 1$, i.e., to *unity* negative-equal susceptivities $\tilde{\sigma}_{se} \approx \pm i + \epsilon$ and $\tilde{\sigma}_{sm} \approx \mp i + \epsilon$ with $\epsilon^2 \ll 1$.

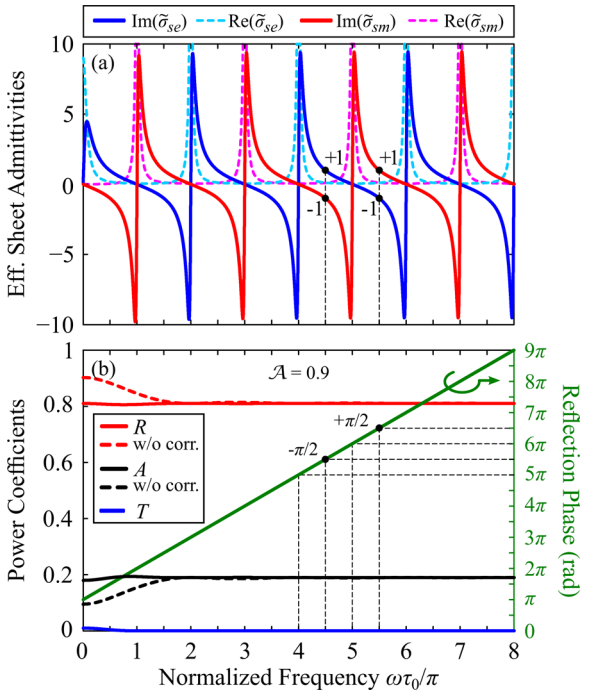

Figure 2. (a) Lorentzian sum recipe of eq 4 for $\mathcal{A} = 0.9$. First four electric ($\tilde{\omega}_{e,k} \approx 2k$) and magnetic ($\tilde{\omega}_{m,k} \approx 2k + 1$) resonances. Note the corrected electric Drude ($k = 0$) term for supplying proper loss at DC. (b) Metasurface response: The reflection amplitude is flat and the phase linear. The latter relies on characteristic points of unity negative-equal susceptivities ($\tilde{\sigma}_{se} \approx \pm i + \epsilon$, $\tilde{\sigma}_{sm} \approx \mp i + \epsilon$), which lead to a reflection phase $\mathrm{Arg}(r) = \mp\pi/2$ occurring at the midpoints between resonances ($\tilde{\omega} \approx k + 1/2$).

TOLERANCE ON INCIDENCE ANGLE—ANGULAR BANDWIDTH

Let us now investigate the effect of incidence angle on the recipe described by eq 4 and the corresponding electromagnetic response. This is important for assessing the angular spectrum of wave packets with a finite spatial extent that can be accommodated by the metasurface. We start by noticing that eq 4 is written for the *effective* admittivities. The actual physical admittivities σ_{se} and σ_{sm} can be specified once the desired incidence angle and polarization are determined by utilizing $\tilde{\sigma}_{se} = \zeta\sigma_{se}/2$ and $\tilde{\sigma}_{sm} = \sigma_{sm}/(2\zeta)$. Given that $\zeta^{TE/TM}$ depends on the incidence angle, the recipe holds exactly only for the prescribed angle of incidence unless the physical conductivities are spatially dispersive (nonlocal) with a very specific dispersion that exactly counteracts the angle dependence of $\zeta^{TE/TM}$. Limiting ourselves to local admittivities, some performance degradation is inevitable when the actual incidence angle θ_{act} is

DOI: 10.1021/acsphotonics.7b01415
ACS Photonics 2018, 5, 1101−1107

different from the prescribed θ_{pre}. Specifically, it is easy to show that for TE polarization the electric effective admittivity scales with $\gamma = \sec(\theta_{act})/\sec(\theta_{pre})$ and the magnetic effective admittivity with $1/\gamma$. The opposite holds for TM polarization. This interferes with the recipe of equally strong electric and magnetic resonances (cf. Figure 2a). The reflection amplitude acquires a periodic ripple about the prescribed value $\mathcal{A}$, as demonstrated in Figure 3a for $\gamma = \sqrt{2}$ (TE polarization).

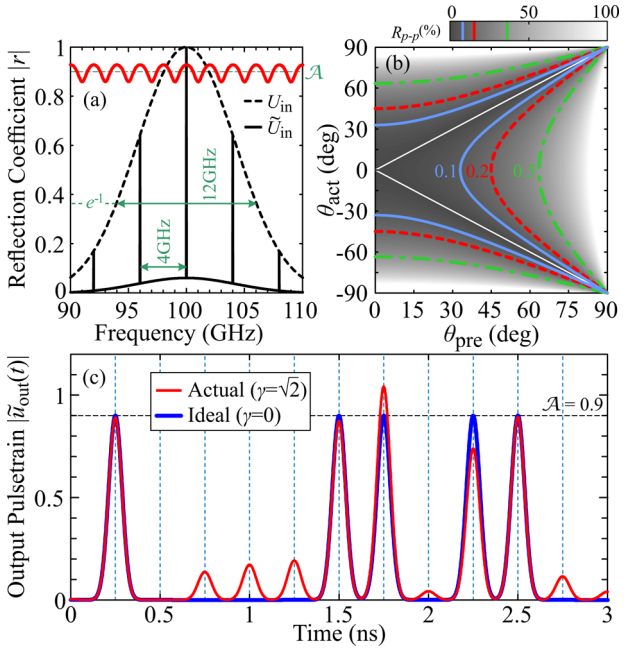

Figure 3. Impact of $\theta_{act} \neq \theta_{pre}$ on pulsed input. (a) Reflection amplitude when $\gamma = \sqrt{2}$ and pulse/pulse-train input spectra. The periodic $r(\omega)$ leads to pulse replicas in the temporal domain. (b) Color-coded fractional peak-to-peak amplitude of R ripple as θ_{act} deviates from θ_{pre}. As R_{p-p} increases, more power is transferred to the pulse replicas. Contours indicate the relative strength of the strongest replica compared to the main pulse. For $\gamma = \sqrt{2}$, R_{p-p} = 15% and the strongest replica is at 0.2 of the main pulse (dashed contour). (c) Output pulse-train. T_{pt} is commensurate with τ_0 (250 and 500 ps, respectively), and pulse replicas fall on the bit positions modifying logical 1's and 0's.

Resistive damping is not masked evenly, leading to a periodically varying absorption, which shows up in the reflection (see Supporting Information). The ripple period is equal to the spacing between two adjacent electric (or magnetic) resonances, i.e., equal to $2\pi/\tau_0$ in ω or $1/\tau_0$ in f. In Figure 3a we have chosen τ_0 = 0.5 ns, leading to a period of 2 GHz.

Next, we study the impact on a broadband input pulse. Consider a single Gaussian pulse $u_{in}(t)$ centered at 100 GHz with a bandwidth of 12 GHz measured at the e^{-1} amplitude points. Multiplication of the pulse spectrum $U_{in}(\omega)$ with the transfer function $r(\omega)$ translates into convolution in the temporal domain. Since the transfer function is periodic, its temporal response is discrete with a period of 0.5 ns, equal to τ_0. As a result, besides the main output pulse at $t = \tau_0$ we get causal pulse replicas at multiples of τ_0 ($t = m\tau_0$, m = 0, 2, 3, ...), with the strongest one at t = 0 (see Supporting Information). They can become detrimental in a pulse-train scenario, especially in real-world conditions with additive noise and jitter (see Supporting Information). Consider for example a pseudorandom pulse-train $\tilde{u}_{in}(t)$ with a period of T_{pt} = 250 ps. The input spectrum, $\tilde{U}_{in}(\omega)$, is depicted in Figure 3a and is characterized by prominent peaks every 4 GHz, i.e., the pulse repetition frequency. In this worst-case scenario where T_{pt} is commensurate with τ_0, pulse replicas fall on the bit positions, modifying both logical 1's and 0's. This can be clearly seen in Figure 3c, where we plot the output pulse-train. For the $\gamma = \sqrt{2}$ case we have considered, the strongest (t = 0) replica is at 0.2 (only 4% intensity) of the main pulse. If the incidence angle deviates even more from the prescribed, replicas become stronger. The fractional peak-to-peak amplitude of the ripple (R_{p-p}) increases (color-coded in Figure 3b), and more energy is transferred to the replicas. In addition, the ripple becomes less sinusoidal with higher-order replicas coming into play (see Supporting Information). Depending on the application, only a certain relative strength of the replicas can be tolerated. In turn, this sets upper and lower bounds on the actual incidence angle for a given prescribed angle and defines the minimum spatial extent for an incident wave packet. These bounds are plotted in Figure 3b for characteristic cases of the t = 0 replica relative strength: 0.1, 0.2, 0.5 corresponding to γ = 1.2, $\sqrt{2}$, 2.25, respectively. Obviously, the proposed metasurfaces are characterized by ample angular bandwidth. Only for very steep θ_{pre} angles does the tolerance on θ_{act} deteriorate noticeably since it depends on the secant ratio γ.

REALISTIC IMPLEMENTATION WITH FEW LORENTZIAN RESONANCES

The recipe described by the infinite sums in eq 4 guarantees perfectly flat reflection amplitude and exactly linear reflection phase for arbitrarily wide bandwidths. In practice, however, one can implement only a limited number of resonances on the metasurface. Figure 4 examines the effect of truncating the infinite sum to a practical number of terms keeping three electric and four magnetic resonances around the normalized frequency $\tilde{\omega}$ = 100. Their positions are marked in Figure 4c with circles and crosses, respectively. Obviously, truncation results in a finite reflection bandwidth, as shown in Figure 4c. The full width half-maximum (fwhm) of the reflection band is ~6. In addition, it interferes with the antimatching condition due to the absence of lower- and higher-order resonances (see Supporting Information). Consequently, the reflection amplitude and group delay slightly deviate from the prescribed values, predominantly near the band edges (Figure 4c,d).

Let us consider now an incident pulse with a spectral bandwidth of 4 measured at the e^{-2} intensity points (Figure 4c) impinging on the metasurface. The corresponding output pulse is depicted in Figure 4b. It is somewhat shifted and attenuated compared to the ideal case of no truncation since, on average, R and τ_g are slightly lower than prescribed (Figure 4c,d). However, there is negligible broadening or distortion, as can be seen by properly shifting and scaling the ideal output pulse. Importantly, it is not the nonideal response in the reflection band, but rather the finite bandwidth that constitutes the bottleneck of the truncated recipe performance; incident pulses with higher bandwidths would simply experience windowing (see Supporting Information).

Finally, we study the combined effect of sum truncation and $\theta_{act} \neq \theta_{pre}$. We consider a pulse-train impinging on the metasurface at an incidence angle different from the prescribed. The pulse-train period is set to T_{pt} = 700 ps and τ_0 = 500 ps; they are incommensurate, meaning that pulse replicas will not

DOI: 10.1021/acsphotonics.7b01415
ACS Photonics 2018, 5, 1101−1107

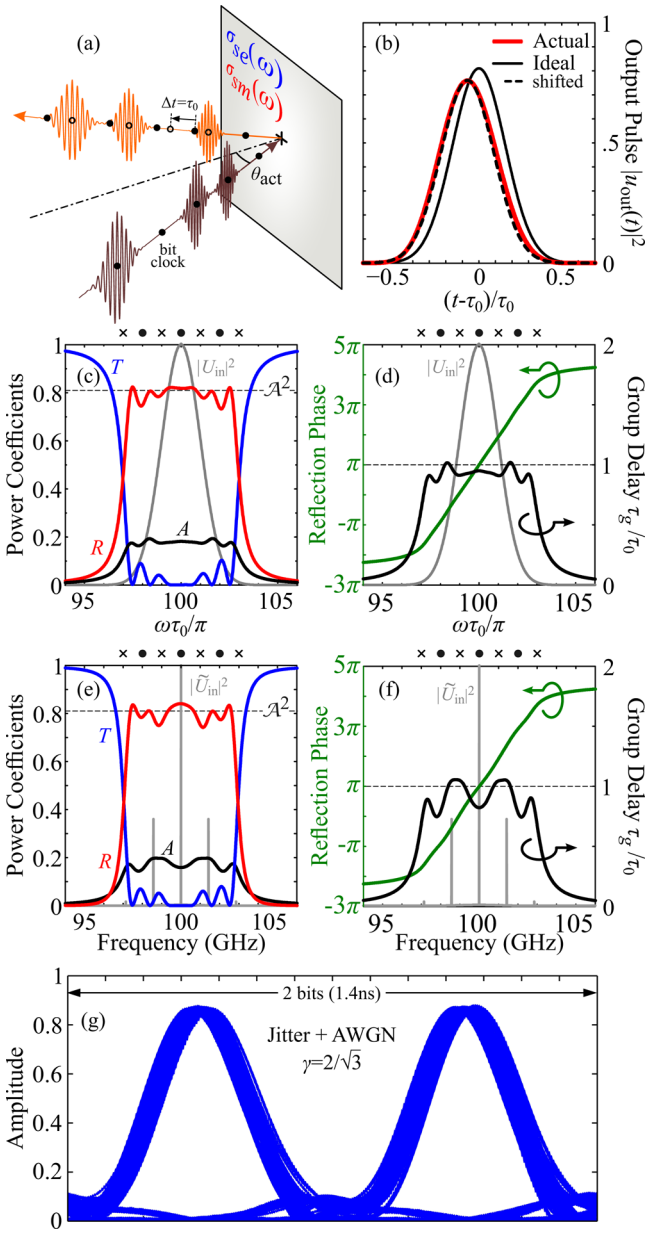

Figure 4. Broadband pulsed input signal impinging on a metasurface with three electric and four magnetic resonances. First case: Single pulse impinging with $\theta_{act} = \theta_{pre}$. (b) Output pulse with negligible broadening or distortion. (c) *R*, *T*, *A* coefficients and input pulse spectrum. Positions of electric and magnetic resonances are marked with solid circles and crosses, respectively. (d) Reflection phase and group delay. Second case: Pulse-train impinging at an incidence angle $\theta_{act} \neq \theta_{pre}$ ($\gamma = 2/\sqrt{3}$). The pulse-train period is T_{pt} = 700 ps and τ_0 is set to 500 ps. (e) *R*, *T*, *A* coefficients and input pulse-train spectrum. (f) Reflection phase and group delay. Notice the added effect of $\theta_{act} \neq \theta_{pre}$. (g) Output eye diagram with jitter and additive white Gaussian noise.

fall on the bit positions (cf. Figure 3c). The metasurface response for $\gamma = 2/\sqrt{3}$ is depicted in Figure 4e,f along with the pulse-train input spectrum. Both reflection amplitude and group delay deviate from their prescribed values. One period of the $1/\tau_0$ = 2 GHz ripple due to $\theta_{act} \neq \theta_{pre}$ is clearly visible in the center of the reflection band, before the effect of truncation also starts contributing near the band edges. The impact on the pulse-train can be assessed by constructing the output eye diagram (Figure 4g). To emulate as realistic a scenario as possible, we have included jitter (normal distribution with a standard deviation of $T_{pt}/50$) and additive white Gaussian noise (signal-to-noise ratio of 20 dB). Even in such real-world conditions, the input pulse-train can be readily recovered as the levels of logical 1 and 0 are clearly distinguishable.

In Figure 4 we have demonstrated how a multiresonant metasurface can be used to reflect a broadband pulse-train imparting a prescribed group delay on the incident pulses. It is worth noting that the number of resonances needed to cover a given bandwidth depends on the desired group delay. For example, the seven resonances in Figure 4a can cover a 7 GHz bandwidth if the desired group delay is 0.5 ns, or 35 GHz if it is 0.1 ns. Finally, we stress that the proposed approach is general and not limited to any particular region of the electromagnetic spectrum. For example, broadband tunable delay components are particularly useful in wavelength-division-multiplexed telecommunication systems operating at infrared wavelengths. In such cases, providing the tunable time delay over broad bandwidths while preserving signal integrity, as demonstrated in Figure 4g for Gbit/s transmission rates, is of utmost importance. The examples in Figures 3 and 4 refer to GHz carrier frequencies, since implementing multiple electric and magnetic resonances on the metasurface unit cell should be easier compared to the infrared or optical regime, allowing for a first demonstration. For example, one could employ printed elements on multisided circuit boards as done in refs 7 and 27.

For the meta-atoms, one potential choice is the cut-wire pair, which supports closely spaced electric and magnetic resonances. By tuning the geometry, the resonant frequencies can be continuously varied so that the resonances progressively approach and ultimately cross,[37] providing a valuable degree of freedom. Then, arranging multiple cut-wire pairs inside the unit cell in an appropriate topology and tuning the system parameters to accurately space the resonances and balance their strength could offer a route to a physical implementation of the proposed concept. Apart from cut-wire pairs, practically any resonant meta-atom studied in metamaterials and metasurfaces research could be investigated for this purpose, since they have been shown to result in Lorentzian spectral features in the electric and/or magnetic admittivities, as required by the derived recipe (eq 4). These include plasmonic resonances in variants of cut-wires, split ring resonators and fishnet structures, as well as electric and magnetic resonant Mie modes in dielectric particles. Finally, one can use one meta-atom for each resonance or resonance pair or, instead, rely on multiresonant meta-atoms for either the electric or magnetic response.

CONCLUSION

In conclusion, we have shown that multiresonant metasurfaces can greatly exceed the typical limitation of a 0−2π imparted phase modulation. For operation in reflection, the proper way of arranging the resonances is interleaving electric and magnetic resonances, leading to an accumulative monotonic reflection phase across their aggregate bandwidth. Combining this principle with an admittivity antimatching condition that zeroes out transmission and requiring an exactly linear reflection phase, we have successfully demonstrated metasurfaces that can perfectly reflect a broadband pulse-train imparting a specified group delay on the incident pulses.

To assess the performance of the proposed metasurfaces, we have thoroughly studied their tolerance on incidence angle and

DOI: 10.1021/acsphotonics.7b01415
ACS Photonics 2018, 5, 1101−1107

found that they are characterized by ample angular bandwidth. In addition, we have shown that few resonances can accommodate a broadband input pulse-train without pulse distortion, indicating the potential of our approach for practical applications. Finally, we have established their performance for realistic Gbit/s transmission rates in real-world conditions with timing and amplitude noise.

In this paper, we have solved the physical problem of establishing the theoretical principles and foundations for obtaining an arbitrarily broadband linear reflection phase from a metasurface. A next step would be to engineer an actual implementation of a metasurface that approximates the derived surface admittivities by appropriately combining discrete meta-atoms. This is a complex engineering task that will be the subject of future work.

Our results highlight that ubiquitous phase modulation and dispersion engineering operations (such as tunable group delay, dispersion compensation, pulse compression, and slow light effects), which customarily rely on bulky resonators, can be instead performed across the deeply subwavelength thickness of a metasurface. Thus, they can push metasurfaces into uncharted territories of broadband temporal applications, previously considered a privilege of three-dimensional systems relying on phase accumulation.

■ ASSOCIATED CONTENT

Supporting Information

The Supporting Information is available free of charge on the ACS Publications website at DOI: 10.1021/acsphotonics.7b01415.

Detailed account of the physical recipe derivation, assessment of the effect of exceeding the available spectral and angular bandwidth, and examination of real-world pulse-train scenarios with timing and amplitude noise. (PDF)

■ AUTHOR INFORMATION

Corresponding Author

*E-mail: otsilipakos@iesl.forth.gr.

ORCID

Odysseas Tsilipakos: 0000-0003-4770-0955

Notes

The authors declare no competing financial interest.

■ ACKNOWLEDGMENTS

Work at Ames Laboratory was supported by the Department of Energy (Basic Energy Sciences, Division of Materials Sciences and Engineering) under contract no. DE-AC02-07CH11358. Work at FORTH was supported by the European Research Council under ERC Advanced Grant no. 320081 (project PHOTOMETA) and the European Union's Horizon 2020 Future Emerging Technologies call (FETOPEN-RIA) under grant agreement no. 736876 (project VISORSURF).

■ REFERENCES

(1) Landy, N. I.; Sajuyigbe, S.; Mock, J. J.; Smith, D. R.; Padilla, W. J. Perfect metamaterial absorber. *Phys. Rev. Lett.* **2008**, *100*, 207402.

(2) Fan, Y.; Shen, N.-H.; Koschny, T.; Soukoulis, C. M. Tunable terahertz meta-surface with graphene cut-wires. *ACS Photonics* **2015**, *2*, 151−156.

(3) Dastmalchi, B.; Tassin, P.; Koschny, T.; Soukoulis, C. M. Strong group-velocity dispersion compensation with phase-engineered sheet metamaterials. *Phys. Rev. B: Condens. Matter Mater. Phys.* **2014**, *89*, 115123.

(4) Tassin, P.; Zhang, L.; Koschny, T.; Economou, E. N.; Soukoulis, C. M. Low-loss metamaterials based on classical electromagnetically induced transparency. *Phys. Rev. Lett.* **2009**, *102*, 053901.

(5) Yu, N.; Genevet, P.; Kats, M. A.; Aieta, F.; Tetienne, J.-P.; Capasso, F.; Gaburro, Z. Light Propagation with Phase Discontinuities: Generalized Laws of Reflection and Refraction. *Science* **2011**, *334*, 333−337.

(6) Ni, X.; Emani, N. K.; Kildishev, A. V.; Boltasseva, A.; Shalaev, V. M. Broadband light bending with plasmonic nanoantennas. *Science* **2012**, *335*, 427−427.

(7) Pfeiffer, C.; Grbic, A. Metamaterial Huygens' Surfaces: Tailoring Wave Fronts with Reflectionless Sheets. *Phys. Rev. Lett.* **2013**, *110*, 197401.

(8) Selvanayagam, M.; Eleftheriades, G. V. Discontinuous electromagnetic fields using orthogonal electric and magnetic currents for wavefront manipulation. *Opt. Express* **2013**, *21*, 14409−14429.

(9) Monticone, F.; Estakhri, N. M.; Alù, A. Full Control of Nanoscale Optical Transmission with a Composite Metascreen. *Phys. Rev. Lett.* **2013**, *110*, 203903.

(10) Sun, S.; Yang, K.-Y.; Wang, C.-M.; Juan, T.-K.; Chen, W. T.; Liao, C. Y.; He, Q.; Xiao, S.; Kung, W.-T.; Guo, G.-Y.; Zhou, L.; Tsai, D. P. High-efficiency broadband anomalous reflection by gradient meta-surfaces. *Nano Lett.* **2012**, *12*, 6223−6229.

(11) Pors, A.; Nielsen, M. G.; Eriksen, R. L.; Bozhevolnyi, S. I. Broadband focusing flat mirrors based on plasmonic gradient metasurfaces. *Nano Lett.* **2013**, *13*, 829−834.

(12) Decker, M.; Staude, I.; Falkner, M.; Dominguez, J.; Neshev, D. N.; Brener, I.; Pertsch, T.; Kivshar, Y. S. High-efficiency dielectric Huygens' surfaces. *Adv. Opt. Mater.* **2015**, *3*, 813−820.

(13) Asadchy, V. S.; Ra'di, Y.; Vehmas, J.; Tretyakov, S. A. Functional Metamirrors Using Bianisotropic Elements. *Phys. Rev. Lett.* **2015**, *114*, 095503.

(14) Achouri, K.; Salem, M. A.; Caloz, C. General metasurface synthesis based on susceptibility tensors. *IEEE Trans. Antennas Propag.* **2015**, *63*, 2977−2991.

(15) Yu, Y. F.; Zhu, A. Y.; Paniagua-Domínguez, R.; Fu, Y. H.; Luk'yanchuk, B.; Kuznetsov, A. I. High-transmission dielectric metasurface with 2π phase control at visible wavelengths. *Laser Photonics Rev.* **2015**, *9*, 412−418.

(16) Estakhri, N. M.; Argyropoulos, C.; Alù, A. Graded metascreens to enable a new degree of nanoscale light management. *Philos. Trans. R. Soc., A* **2015**, *373*, 20140351.

(17) Epstein, A.; Eleftheriades, G. V. Synthesis of Passive Lossless Metasurfaces Using Auxiliary Fields for Reflectionless Beam Splitting and Perfect Reflection. *Phys. Rev. Lett.* **2016**, *117*, 256103.

(18) Asadchy, V. S.; Albooyeh, M.; Tcvetkova, S. N.; Díaz-Rubio, A.; Ra'di, Y.; Tretyakov, S. A. Perfect control of reflection and refraction using spatially dispersive metasurfaces. *Phys. Rev. B: Condens. Matter Mater. Phys.* **2016**, *94*, 075142.

(19) Asadchy, V. S.; Wickberg, A.; Díaz-Rubio, A.; Wegener, M. Eliminating scattering loss in anomalously reflecting optical metasurfaces. *ACS Photonics* **2017**, *4*, 1264−1270.

(20) Díaz-Rubio, A.; Asadchy, V. S.; Elsakka, A.; Tretyakov, S. A. From the generalized reflection law to the realization of perfect anomalous reflectors. *Sci. Adv.* **2017**, *3*, e1602714.

(21) Estakhri, N. M.; Neder, V.; Knight, M. W.; Polman, A.; Alù, A. Visible Light, Wide-Angle Graded Metasurface for Back Reflection. *ACS Photonics* **2017**, *4*, 228−235.

(22) Grady, N. K.; Heyes, J. E.; Chowdhury, D. R.; Zeng, Y.; Reiten, M. T.; Azad, A. K.; Taylor, A. J.; Dalvit, D. A. R.; Chen, H.-T. Terahertz metamaterials for linear polarization conversion and anomalous refraction. *Science* **2013**, *304*, 1304−1307.

(23) Kruk, S.; Hopkins, B.; Kravchenko, I. I.; Miroshnichenko, A.; Neshev, D. N.; Kivshar, Y. S. Broadband highly efficient dielectric metadevices for polarization control. *APL Photonics* **2016**, *1*, 030801.

DOI: 10.1021/acsphotonics.7b01415
ACS Photonics 2018, 5, 1101−1107

(24) Sounas, D. L.; Kodera, T.; Caloz, C. Electromagnetic modeling of a magnetless nonreciprocal gyrotropic metasurface. *IEEE Trans. Antennas Propag.* **2013**, *61*, 221−231.
(25) Hadad, Y.; Sounas, D. L.; Alù, A. Space-time gradient metasurfaces. *Phys. Rev. B: Condens. Matter Mater. Phys.* **2015**, *92*, 100304R.
(26) Estakhri, N. M.; Alù, A. Recent progress in gradient metasurfaces. *J. Opt. Soc. Am. B* **2016**, *33*, A21−A30.
(27) Epstein, A.; Eleftheriades, G. V. Huygens' metasurfaces via the equivalence principle: design and applications. *J. Opt. Soc. Am. B* **2016**, *33*, A31−A50.
(28) Minovich, A. E.; Miroshnichenko, A. E.; Bykov, A. Y.; Murzina, T. V.; Neshev, D. N.; Kivshar, Y. S. Functional and nonlinear optical metasurfaces. *Laser Photonics Rev.* **2015**, *9*, 195−213.
(29) Hsiao, H.-H.; Chu, C. H.; Tsai, D. P. Fundamentals and Applications of Metasurfaces. *Small Methods* **2017**, *1*, 1600064.
(30) Ginis, V.; Tassin, P.; Koschny, T.; Soukoulis, C. M. Broadband metasurfaces enabling arbitrarily large delay-bandwidth products. *Appl. Phys. Lett.* **2016**, *108*, 031601.
(31) These quantities are related to the surface susceptibilities through $\sigma_{se} = -i\omega\epsilon\chi_{se}$, $\sigma_{sm} = -i\omega\mu\chi_{sm}$ and can be also found as Y_{se} and Z_{sm} in the literature.
(32) Tassin, P.; Koschny, T.; Soukoulis, C. M. Effective material parameter retrieval for thin sheets: Theory and application to graphene, thin silver films, and single-layer metamaterials. *Physica B* **2012**, *407*, 4062−4065.
(33) Holloway, C. L.; Kuester, E. F.; Dienstfrey, A. Characterizing Metasurfaces/Metafilms: The Connection Between Surface Susceptibilities and Effective Material Properties. *IEEE Antennas Wirel. Propag. Lett.* **2011**, *10*, 1507−1511.
(34) One can easily verify that a three-dimensional system that can satisfy these scattering amplitudes is a matched ($\epsilon_r = \mu_r$) slab on top of a reflecting mirror. In this case, group delay originates from phase accumulation in the slab, instead of (effective) material dispersion. Specifically, τ_0 equals $2dn/c$, where $n = \sqrt{\epsilon_r\mu_r}$ is the slab refractive index, d is the slab thickness, and c the velocity of light in vacuum.
(35) Ra'di, Y.; Asadchy, V. S.; Tretyakov, S. A. Tailoring reflections from thin composite metamirrors. *IEEE Trans. Antennas Propag.* **2014**, *62*, 3749−3760.
(36) Estakhri, N. M.; Alù, A. Wave-front transformation with gradient metasurfaces. *Phys. Rev. X* **2016**, *6*, 041008.
(37) Zhou, J.; Economou, E. N.; Koschny, T.; Soukoulis, C. M. Unifying approach to left-handed material design. *Opt. Lett.* **2006**, *31*, 3620−3622.

DOI: 10.1021/acsphotonics.7b01415
ACS Photonics 2018, 5, 1101−1107